



## Research Article

# Research on the performance of hydraulic vibratory hammer with coupled dynamic model



Gao Lulu<sup>1,2</sup> · Wang Dongyue<sup>1</sup> · Wang Shite<sup>1</sup>

Received: 17 February 2022 / Accepted: 25 August 2022

Published online: 06 September 2022

© The Author(s) 2022 [OPEN](#)

## Abstract

Hydraulic vibratory hammer is a key equipment during piling process, and mechanical, hydraulic part of the hammer and workload are coupled with each other during operation. The vibration performance depends on the design parameters and the driving system. In order to investigate the vibration performance, a coupled dynamic model is established for hydraulic vibratory hammer, in which the mechanical model of hammer, hydraulic model for driving, and the model of workload are included. The field test was carried out to validate the dynamic model under idle and operating conditions. Pressure and flow of the hydraulic driving system and acceleration of the mechanical part were obtained during different test conditions. The results of test and simulation were analyzed in time and frequency domain to validate the coupled dynamic model. Then, effects of different eccentric block parameters on the vibration performance were investigated based on the validated model, including radius, thickness, and angle of the eccentric block. Further the design parameters of optimal vibration performance of the hammer are obtained under the constraints of hammer structure, in which the angle is 90°, thickness is 190 mm, and radius is 175 mm.

## Article Highlights

- (1) We established a coupled dynamic model of the hydraulic vibratory hammer, including the mechanical model of hammer, hydraulic model for driving, and the simplified model of workload;
- (2) The field test is proceeded to validate the model under idle and operating condition; the dynamic response of the mechanical part and hydraulic driving part is analyzed in time and frequency domain;
- (3) The performance of the hammer is analyzed with the coupled dynamic model, in which better performance of the hammer is obtained. The model-based method also provides a rapid and economical solution for the performance optimization of the hammer.

**Keywords** Vibratory hammer · Coupled dynamic model · Vibration performance · Eccentric block

**JEL Classification** 70E55

✉ Gao Lulu, gaolulu@ustb.edu.cn | <sup>1</sup>School of Mechanical Engineering, University of Science and Technology Beijing, Beijing 100083, China. <sup>2</sup>Shunde Graduate School, University of Science and Technology Beijing, Foshan, Guangdong 528399, China.



SN Applied Sciences

(2022) 4:259

| <https://doi.org/10.1007/s42452-022-05144-3>

SN Applied Sciences  
A **SPRINGER NATURE** journal

## 1 Introduction

As a kind of piling equipment, the hydraulic vibratory hammer can drive different prefabricated piles, including steel, pipe, and concrete. It has been widely applied in construction industry and costal engineering [1, 2] with the advantages of low noise level, high efficiency, and powerful characteristics [1, 3–5]. The vibratory hammer drives piles with high frequency exciting force, which originated from the hydraulic-powered symmetrical eccentric mass, and the work efficiency is decided by the vibration performance [6].

Due to the coupling effects of pile and surrounding soil during working process, much attention had been paid on the dynamics of pile and soil. Some overall models of mechanical–electric–hydraulic–pile–soil were also considered, while the dynamic characteristics of the hammer was ignored and only the influence of the leakage of the hydraulic drive motor on the synchronization of the eccentric mass were considered [5]. Zhang established a hysteretic nonlinear model of sandy soil vibratory pile sinking capacity and comprehensively analyzed the influence of soil and other factors on the pile sinking capacity [7]. Although the characteristic of load and piles affects the performance of hydraulic vibratory hammer significantly during working process, the dynamic vibration characteristics of the hammer, which originated from the coupling mechanical and hydraulic parts, are also crucial.

Vibration of the hammer normally comes from the rotation of the eccentric mass, for which different theories exist [8], while the vibration performance of hydraulic vibratory hammer is always ignored [9, 10]. Vibration performance of the hammer depends on the driving system, i.e., the hydraulic-powered system, and the dynamic responses of involved mechanical structures. Liu analyzed the relationship between the amplitude and the eccentric moment of the eccentric mass with a 1DOF dynamic model of the hammer, in which the hammer was considered as a rigid body [11]. Li et al. [12] established a 2DOF dynamic model of hydraulic vibratory hammer, in which the dynamic characteristics of the hammer body and the damping structure were involved. And then dynamic responses of the hammer, including the excitation force, frequency, and the piling performance, were investigated with simulation. The results showed that the structure characteristic of the hammer affected the amplitude of vibration and the excitation force and the frequency played an important role in the working performance. However, the driving system of the hammer was always ignored, and the models of hydraulic parts were not considered. And the

performance of hydraulic system was not involved during the working performance analysis of the hammer. Zhou [13] et al. studied the performance of a vibratory hammer with a AMESim model, in which the models of hydraulic cylinder, pipeline, and accumulator were included and the effects of hydraulic system parameters on the vibratory performance of the hammer were investigated with simulation. However, the working principle of the target hammer is different from the conventional hammer. The former one produced the excitation force with a reciprocating cylinder, and the cylinder was controlled with an alternating flow device. The other accessories of the system ensured the safe and efficient operating of the hammer. The conventional hammer was driven with a hydraulic motor, and the excitation force originated from the rotation of eccentric mass [14–16].

Above all, much attention had been paid to the effects of pile and soil properties [17, 18], and the structures of the hammer were also considered [3, 5, 6]. And some researches had focused on the hydraulic drive motor, while the involved mechanical and workload parts were not involved integrally. In addition, the vibratory hammer will pass through the resonance region of the system, which will produce noise pollution and damage to the mechanical structure, and it is closely related to the overall dynamic responses of these coupled hydraulic-mechanical structures. And the compact of hammer also affect the parts of hydraulic system and surroundings of working environment [19, 20], If the dynamic responses and vibration performance of the hammer are evaluated with field test, it will take time and efforts [21]. The coupled dynamic model would be crucial to evaluate the performance of hydraulic vibratory hammer economically and effectively. In this paper, a coupled dynamic model of hydraulic vibratory hammer is established to evaluate the vibration performance, and the field test in different conditions are carried to validate the coupled model. And the influence of structural parameters on vibration performance of the hammer is discussed with the coupled models, which would be effective to improve efficiency of the hammer.

The rest of this paper is organized as follows. In Sect. 2, the coupled dynamic model, including mechanical model, hydraulic model, and workload model, is established. The idle and operating field tests of hydraulic vibratory hammer is carried in Sect. 3. Then the time and frequency domain results of the coupled dynamic model and the field test are compared in Sect. 4. In Sect. 5, the performance of the hammer is evaluated with coupled dynamic model, and the comparing results of different operating conditions are discussed. Lastly, conclusions and an outlook future work are given.

## 2 Coupled dynamic model

The hydraulic vibratory hammer is always installed on a modified excavator, as shown in Fig. 1a, in which the manipulator is used to connect hammer and boom of excavator. And the hammer can be considered as a coupled dynamic model, as shown in Fig. 1b. It is driven with a hydraulic motor, and the hydraulic flow is provided by the excavator, and is regulated with a valve to change the speed of the motor. The eccentric mass in the hammer body, which is driven by motor, rotates to produce the excitation. The mechanical parts, including cradle, frame, and body, are connected by spring and damping blocks, while the body, clamp, and the pile are connected rigidly. During the piling process, the excitation drives the mechanical parts including the pile to cope with workload, which comes from the action of pile and soil, and the workload produce resistance torque counteracting the hydraulic motor through the mechanical parts. Therefore, model of the hammer can be considered as three models, i.e., mechanical model, hydraulic model, and workload model.

### 2.1 Mechanical model of the hammer

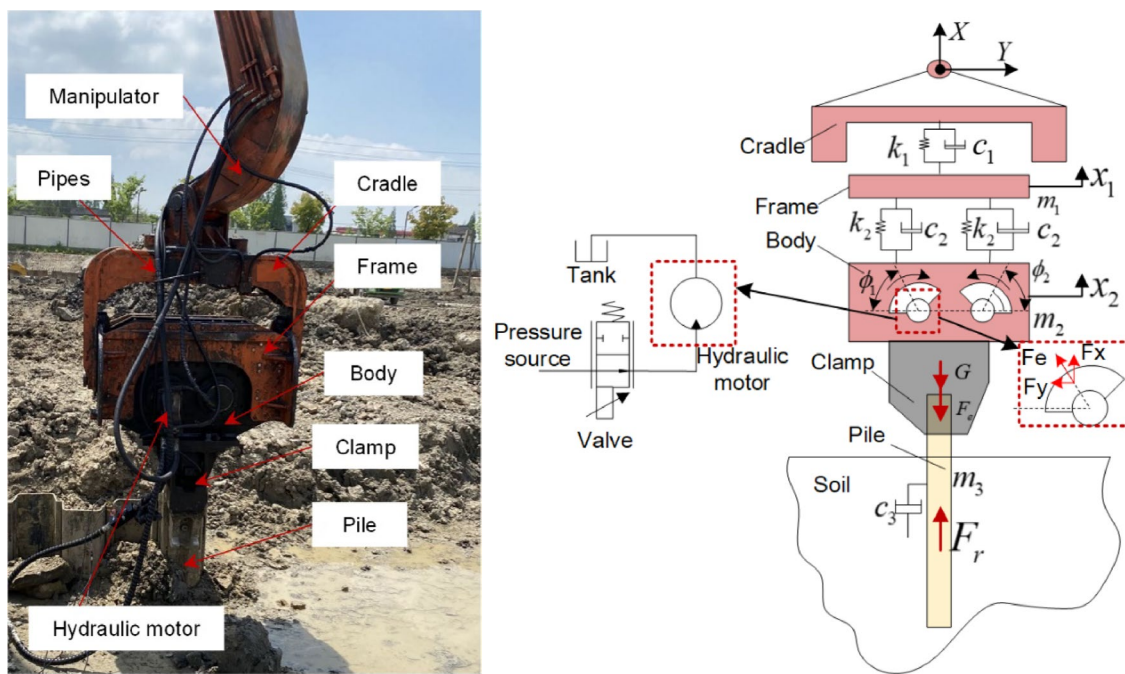
As the basic structure of the hammer, the mechanical parts contain the mechanical cradle, frame, body and clamp. The

model of the mechanical parts can be considered as a 3 degrees of freedom (DOF) dynamic model, as shown in Fig. 1b. The cradle of the hammer is always installed on the manipulator, which is connected with the excavator. It means that the cradle is fixed with the manipulator. During the piling process, the hammer is pressed into the hole with uniform velocity by the manipulator, and the acceleration of this motion is far less than the eccentric-excited acceleration of the hammer body. In the idle condition, the hammer was driven without workload and downward motion. According to Newton's second law, the dynamic model can be given by:

$$m_1 \ddot{x}_1 + (c_1 + c_2) \dot{x}_1 - c_2 \dot{x}_2 + (k_1 + k_2)x_1 - k_2 x_2 = 0 \quad (1)$$

$$(m_2 + m_3) \ddot{x}_2 + (c_2 + c_3) \dot{x}_2 - c_2 \dot{x}_1 - k_2 x_1 = F_e - F_r \quad (2)$$

where  $x_1$  and  $x_2$  are the displacement of frame and body, respectively.  $m_1$ ,  $m_2$ , and  $m_3$  are the mass of frame, body and the pile, respectively. And  $k_1$  and  $c_1$  are the stiffness and damping between cradle and frame, respectively;  $k_2$  and  $c_2$  are the stiffness and damping between frame and body of the hammer, respectively;  $c_3$  is the damping between pile and soil.  $F_r$  is the resistance of pile during working, which originates from workload. The direction of the involved forces is the vertical direction in X-axis for the coordination in Fig. 1(b).  $F_e$  is the exciting force from the rotation of the eccentric mass, which can be given by [12]:



(a) Main structure of the hammer (b) Coupled dynamic model of the hammer

Fig. 1 Physical and coupled dynamic model of hydraulic vibratory hammer

$$\vec{F}_e = \vec{F}_y + \vec{F}_x \tag{3}$$

$$\vec{F}_x = F_1 \sin \varphi_1 - F_2 \sin \varphi_2 \tag{4}$$

$$\vec{F}_y = F_1 \cos \varphi_1 + F_2 \cos \varphi_2 \tag{5}$$

$$F_1 = F_2 = mr\omega^2 \tag{6}$$

$$\varphi_1 = -\varphi_2 = \omega t \tag{7}$$

where the index 1 and 2 indicate the active and passive eccentric mass, respectively.  $m$  and  $r$  are the mass and eccentric distance, respectively.  $\varphi$  and  $\omega$  are the rotation angle and angular velocity of eccentric mass, since the two shafts of eccentric mass rotate synchronously and inversely, the direction of angle and angular speed are opposite. Then we can obtain the exciting force [5]:

$$F_e = 2mr\omega^2 \sin \varphi_1 \tag{8}$$

The angle and angular velocity can be obtained by dynamic model of eccentric mass, which can be expressed as:

$$J_1 \ddot{\omega}_1 = T - T_2 - \dot{\omega}_1 c_e \tag{9}$$

$$J_2 \ddot{\omega}_2 = T_2 - \dot{\omega}_2 c_e \tag{10}$$

$$\omega_1 = -\omega_2 \tag{11}$$

where  $J_1$ , and  $J_2$  are the moment of inertia for eccentric mass,  $T$  is the driving force of hydraulic motor,  $T_2$  is the driving torque of passive eccentric mass.  $c_e$  is the rotational damping. The driving torque will be given in the hydraulic model.

The mechanical model of the hammer was obtained by substituting Eqs. (3)–(11) into (1)–(2).

### 2.2 Hydraulic model

As shown in Fig. 1b (simplified schematic) and Fig. 2 (detailed schematic), the hydraulic model contains the models of hydraulic valve, motor, inlet and outlet pipes. The valve, which is the key control component, decides the inlet flow of the system. The inlet flow is obtained from a flow sensor during experiments. The hydraulic motor is connected with the hydraulic pump by a very long pipeline, and the flow wave is weak. So, we focus on the model of valve, motor, and pipes, in which the model of hydraulic valve and motor can be given by:

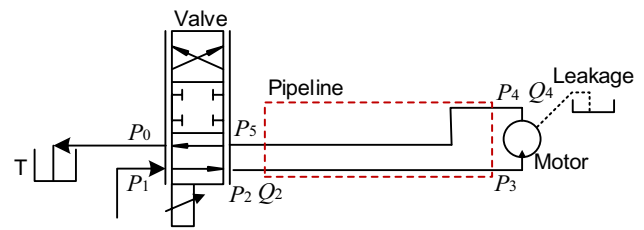


Fig. 2 Schematic diagram of hydraulic model for driving system

$$Q_2 = AC_d \sqrt{2(p_1 - p_2) / \rho} \tag{10}$$

$$Q_0 = AC_d \sqrt{2(p_5 - p_0) / \rho} \tag{11}$$

$$Q_2 = Q_{in} + Q_4 \tag{12}$$

$$Q_{in} = nD / \eta_v \tag{13}$$

$$T = D(p_3 - p_4) \eta_m \tag{14}$$

where  $Q_2$ ,  $Q_0$ ,  $Q_{in}$ , and  $Q_4$  are the inlet flow, out flow of valve, inlet flow and leak flow of the motor, respectively;  $p_0$ ,  $p_1$ ,  $p_2$ ,  $p_5$ ,  $p_3$ , and  $p_4$  are the atmosphere pressure, inlet pressure of valve, out pressure after valve, inlet pressure of return oil, inlet pressure, and out pressure of the motor, respectively;  $A$  is the opening area of valve;  $C_d$  is the discharge parameter;  $\rho$  is the density of hydraulic oil;  $D$ ,  $n$ ,  $\eta_v$ , and  $\eta_m$  are the capacity, speed, volumetric and mechanical efficiency of the hydraulic motor, respectively. And  $\Delta p$  is the pressure difference between the inlet and outlet port. Normally, the outlet of hydraulic motor is connected with oil tank, which means the outlet pressure is the atmospheric pressure. The inlet pressure can be express as:

$$\dot{p}_i = BQ_i / (\pi r^2 l) (i = 3, 4) \tag{15}$$

where  $B$  is the effective bulk modulus, and it contains the bulk modulus of hydraulic oil and the pipe.  $r$  and  $l$  are the radius and length of inlet pipe.

The Eqs. (10)–(14), give the inlet, outlet flow of the system. And the flow of hydraulic motor can be described in Eqs. (12)–(13). The hydraulic motor is used to drive the eccentric mass, and equilibrium equation of moments can be obtained with Eqs. (14) and (9)–(11).

### 2.3 Workload model

The workload of the hammer originated from the resistance between pile and soil during piling process [22, 23]. The resistance can be given by:

$$\begin{cases} F_r = LfH + F_pA_p \\ f = af_0 \\ F_p = bF_0 \end{cases} \quad (16)$$

where  $F_r$  is the resistance force,  $L$ ,  $f$ ,  $H$  are the perimeter, friction shear stress, and depth of pile, respectively.  $F_p$  and  $A_p$  are resistance in the end and sectional area of pile.  $f_0$  and  $F_0$  are the values of friction and resistance in the end of the pile, and  $a$ ,  $b$  is the corresponding correction factor, which are determined by the condition of piling. In addition, one and the same pile hole was used throughout the test. The friction force is related to the sinking velocity, and the factor  $a$  is decided according to the sinking process. In this paper, the same hole is used during the experiments, the pile is self-sinking. Then the factor  $a$  is 0.2. The resistance force in the end of pile is decided by the crossing area of pile, and the factor  $b$  is used to correct the resistance force.

Then the coupled dynamic model of the hammer was obtained, and it included the mechanical model, hydraulic model, and the workload model. The model should be run in simulation environment, and the results should be validated with field test results. The related contents are arranged in the next section.

### 3 Simulation and field test results

#### 3.1 Simulation and field test setup

The coupled dynamic model was simulated with the co-simulation between AMESim and ADAMS, which was run with 0.005s interval. The frame of simulation was shown in Fig. 3, and the involved parameters were shown in Table 1. As it can be seen from Fig. 3, the mechanical and workload models were simulated in ADAMS, and the hydraulic model was simulated in AMESim. The hydraulic model received the control signal as input control signal, which was the control signal, recorded in field test. The hydraulic model provided the driving torque for mechanical model, and the speed of revolution of mechanical part was fed

**Table 1** Parameters in simulation

Symbol	Parameters	Values
$m_1$	Mass of frame	526 kg
$m_2$	Mass of body	192 kg
$m_3$	Mass of pile	57 kg
$m$	Mass of eccentric block	108 kg
$k_1$	Stiffness between frame and cradle	1e3 N/m
$c_1$	Damping between frame and cradle	2e3 N/m/s
$k_2$	Stiffness between frame and body	1.2e6 N/m
$c_2$	Damping between frame and body	4e4 N/m/s
$J_1, J_2$	Moment of inertia for eccentric mass	1.3 kg m <sup>2</sup>
$c_e$	Rotational damping of eccentric mass	3 N m/(rad/s) N/m/s
$D$	Displacement of hydraulic motor	125 cc/rev
$B$	Effective bulk modulus	4e5 MPa
$r$	Radius of inlet pipe	5/8 in
$l$	Length of inlet pipe	11 m
$L$	Perimeter of pile	1.3 m
$H$	Depth of pile	0–5 m
$a$	Correction factor	0.2
$b$	Correction factor	0.6
$A_p$	Sectional area of pile	0.2 m <sup>2</sup>
$f_0$	Friction values in the end of the pile	4e6 N/ m <sup>2</sup>
$F_0$	Resistance values in the end of the pile	2e5 N/ m <sup>2</sup>

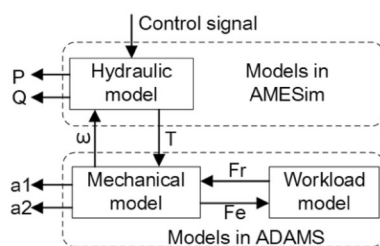


**Fig. 3** Schematic diagram of simulation

back to hydraulic model. Similarly, the mechanical and workload model connected with each other by driving and resistance forces. In order to validate the coupled dynamics comprehensively, the simulation was run at idle and operating condition separately, the workload model was absent in the idle condition and active in the run condition. In addition, the clamp and the pile are disconnected in the idle condition, and the mass of body is also changed.

The parameters in the coupled model include mechanical and hydraulic related. Some parameters are accessible, such as the mass, dimension of pipe, and so on. While some parameters are hard to get, such as the stiffness and damping parameters, and these parameters are also crucial for simulation. The error of these parameters would introduce deviation of the model. In order to calibrate the model, we focused the idle condition, in which only the mechanical and hydraulic models were involved. We proceed different simulations under different parameters according to the test results, and we compared the amplitude and frequency of acceleration and amplitude of pressure during simulation. These involved parameters were tuned to calibrate the coupled model.

The system diagram in field test operation is shown in Fig. 4. Three kinds of sensors were used; accelerometers measure the acceleration signal of the hammer

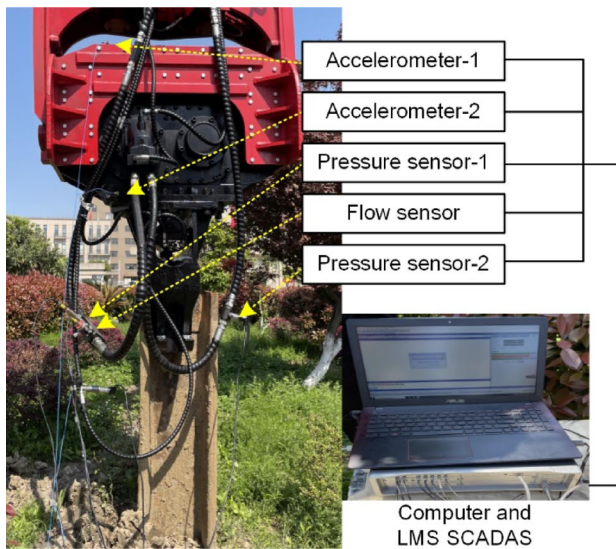
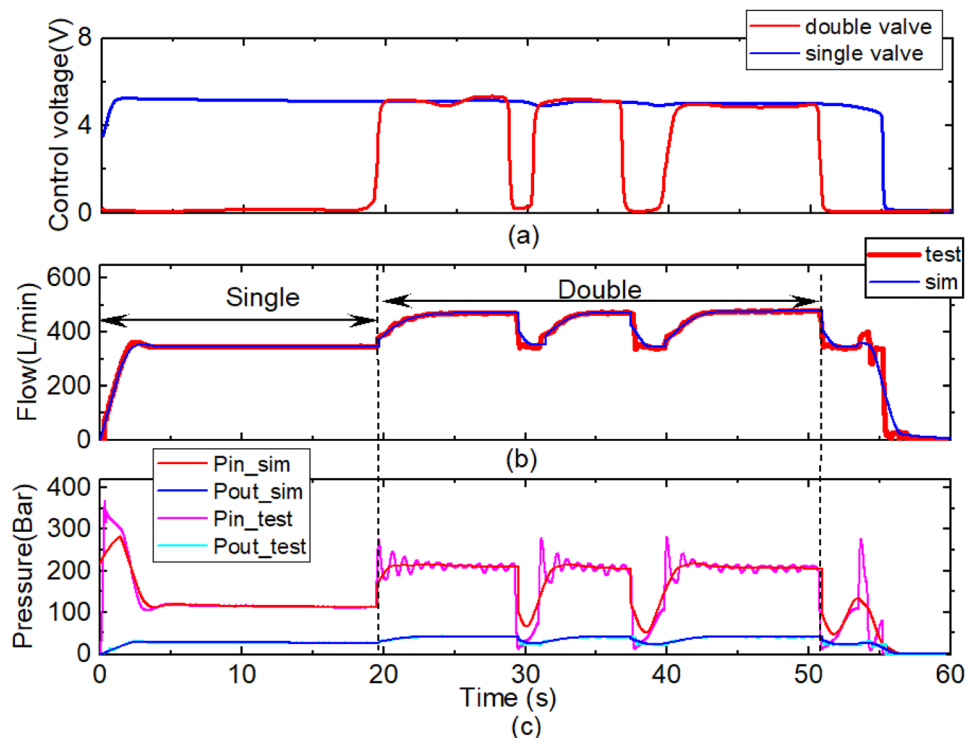


Fig. 4 Field test system diagram

body and frame in vertical direction, and the pressure sensors measure the pressure of hydraulic driving motor in inlet port and outlet port, the flow sensor measures the inlet flow of the motor. A LMS SCADAS record the involved data with a 200 Hz sampling frequency. The field test was processed in idle and operating condition separately, and in the idle condition the clamp released the pile, the hammer is operated to pile in the operating condition.

Fig. 5 Comparing results of flow and pressure in idle condition



The simulation and test results are compared in idle and operating condition. And the data in time and frequency domain is also compared separately.

### 3.2 Idle condition results

The control signal of the valves and results of flow and pressure of simulation and experiments are compared in Fig. 5. The field test lasted 60s, showing the two driving modes of the motor, i.e., single mode and double mode. The single mode, when single valve is open, means the motor was driven with only one pump, and the double mode, when double valve is open, means two pumps in the excavator are used, in which much flow was pumped into the motor. The valves are control by voltage, when the voltage reaches 5 V, the opening area of valve is maximum. As it can be seen from Fig. 5, during the 0–20s, the hammer is started and run as single mode steadily, the steady flow is about 330 L/min, the steady inlet pressure and outlet pressure are 11.5 MPa and 2.9 MPa, respectively. The comparing flow and pressure results of simulation and field test coincide well during the steady single mode, while the trend changes differently during start stage for the comparing simulation and field test results. As it can be seen from the Fig. 5c, the maximum pressure of inlet port is about 35 MPa in the field test, while the maximum pressure is 28 MPa in the simulation. The trend of pressure during start stage depends on two reasons, one is the driving load of eccentric mass, the other is that the

driving motor will experience the resonance frequency region of the mechanical structure of the hammer, which will result in a sharp increase in load. During 20–51s, the hammer is driven with double mode, in which the switch between single and double mode is also involved. During the steady stage of double mode, the inlet flow is about 480 L/min, and the inlet and outlet pressure are about 21 MPa and 4 MPa. The trend of flow and pressure for simulation and test coincide well during steady stage, the inlet pressure changes with slight differences during unsteady stage, the test data changes more sharply, and some ripples appear during steady stage, which is originated from the gap connection between cradle and frame of the hammer. Although the connection is simplified as stiffness and damping blocks in the modeling process, the trend of simulation and test are coincident, which can indicate the dynamic characteristics of the hammer. Therefore, the difference is acceptable. After the double mode, the hammer is switch to single mode and then stopped during 51–0s. The trend of flow and pressure coincide with each other for the data of simulation and test. At the 54s, the pressure increases severely and it is also reflected in the simulation, which is originated from the resonance of the mechanical structure and the driving motor [24, 25]. In addition to the verification of flow and pressure, the structure dynamic responses should also be considered.

We intercepted the acceleration data between 0s–40s of hammer body in vertical direction to verify the dynamic model of hammer, in which the different mode of the hammer is included. The result is shown in Fig. 6. As it can be seen from Fig. 6, the trend of simulation and test coincide well and the amplitude of the acceleration is very close, the differences is originated from the errors between model damping and actual structure. Further, we analyzed the frequency characteristics of single and double mode

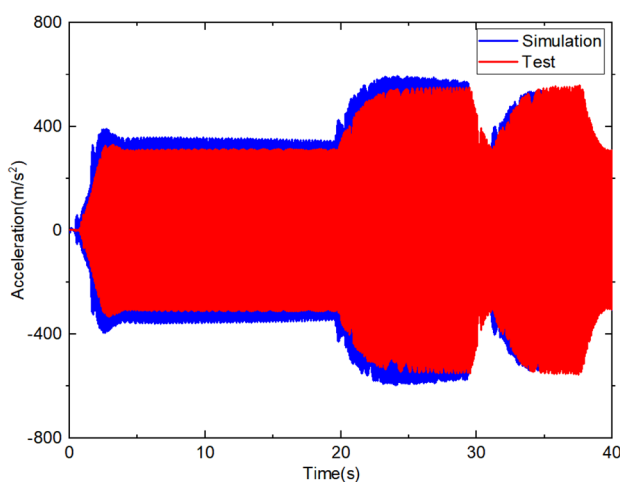


**Fig. 6** Time domain data of body acceleration in vertical direction

during steady stage with fast Fourier transform (FFT) [26], the results are shown in Fig. 7. Figure 7a and b are the comparing results of test and simulation in single mode, respectively, Fig. 7c and d are the comparing results of double mode. According to the results in Fig. 7, the frequency of single and double mode is 42.8 and 57.4 Hz, the amplitude is 260.4  $\text{m/s}^2$  and 430.4  $\text{m/s}^2$ . Although the corresponding data of simulation is different, errors are 2.6% and 4.9% for the frequency and amplitude in single mode steady stage. The correspond error are 2.3% and 2.4% in double mode steady stage.

The frequency at different time during the test is obtained with short time Fourier transform (SFT), results is shown in Fig. 8. Because the data of simulation and test is almost same, we mainly showed and analyzed the results of test. As it can be seen from the figure, the frequency of single and double mode is 42.8 and 57.4 Hz, which is identical to the FFT results. In addition, the trend of frequency at different time is identical to the trend of flow. This is because the hammer is essentially based on forced vibration. And dynamic response frequency of the hammer depends on the excitation frequency, i.e., the frequency of eccentric mass. The eccentric mass is driven by hydraulic motor, and the frequency is related to the speed of motor, which can be obtained with the displacement and flow. The motor of this hammer is a fixed displacement piston motor with 125 cc/rev displacement. Therefore, the trend of flow is identical to SFT results of acceleration data.

### 3.3 Operating condition

After the idle condition, we processed the field test of operating condition. In this condition, the clamp of hammer in connected with a prefabricated steel pile, and the hammer is controlled to pile into the soil. Due to

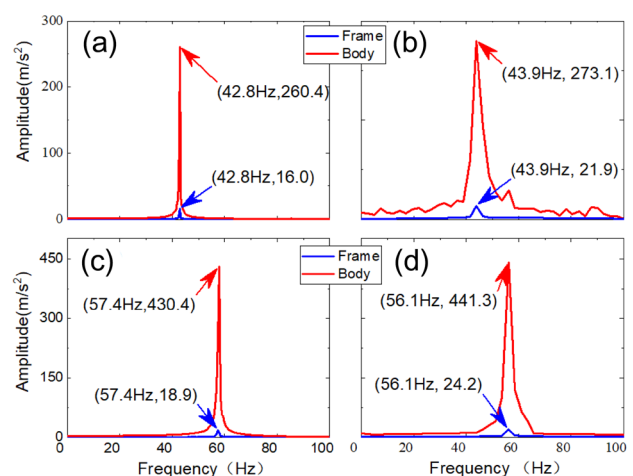
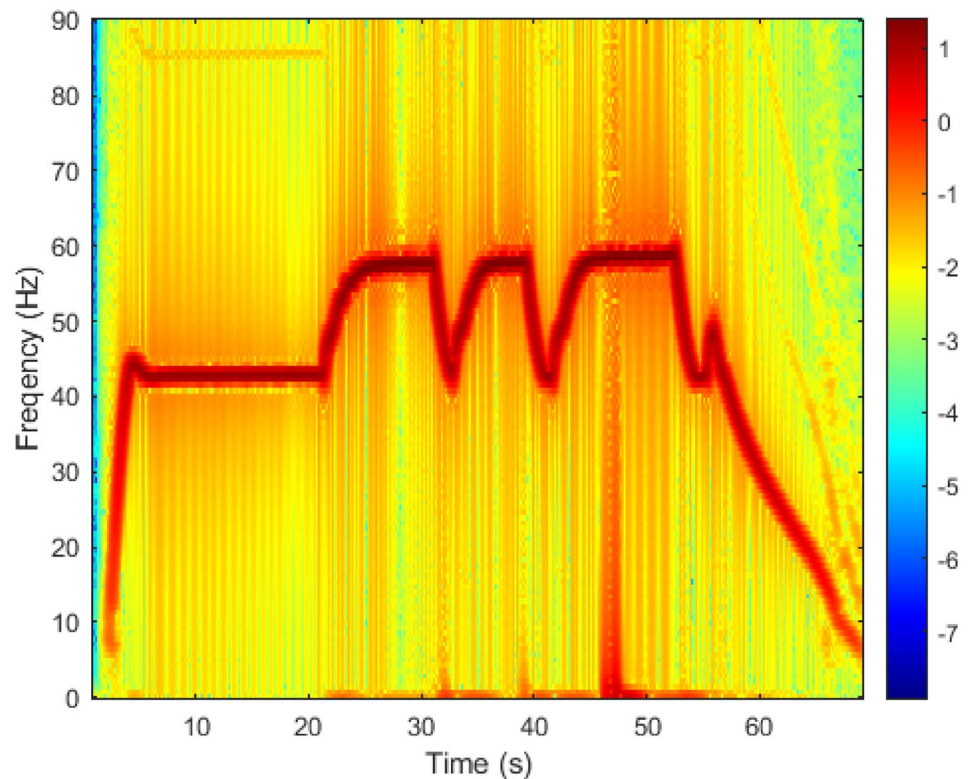


**Fig. 7** FFT results of acceleration in idle condition

**Fig. 8** SFT results of the pressure in idle condition



the limitation of test field, the pile is controlled by an operator piling and lifting up repeatedly during the test, and the control signal of the valves are recorded. The control signal was input to the simulation in the form of time series. The control signal of valves and comparing results of flow and pressure in operating condition are shown in Fig. 9. As it can be seen from the Fig. 9a and b, the test duration is marked as mix and double mode. In the mix mode 10–30s, the motor is driven with switching single and double mode, the inlet flow changes with fluctuation, which is between 280 and 50 L/min. The corresponding inlet pressure changes between 15 and 29 MPa. Although the fluctuation range of simulation and test is different, the trend is identical, and the values of flow and pressure are consistent in a relatively stable range, such as 20s~25s. Identical characteristic appeared in the double mode, during 35–45s. The flow curves of simulation and test almost coincide at these steady stages, the pressure curves are also similar. In addition, the differences between simulation and test appeared at 31–34s, 47–49s, and 57–60s, in which the flow returned to zero in the test and the corresponding flow just reduce and then increased in simulation, and the pressure in Fig. 9c shows the same characteristics. This is because damping, including damping of structure and damping between soil and pile, is greater in the test, and the hammer stop faster when the hydraulic power

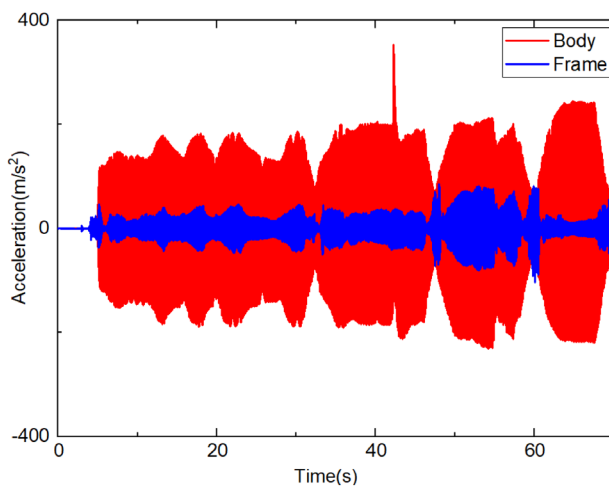
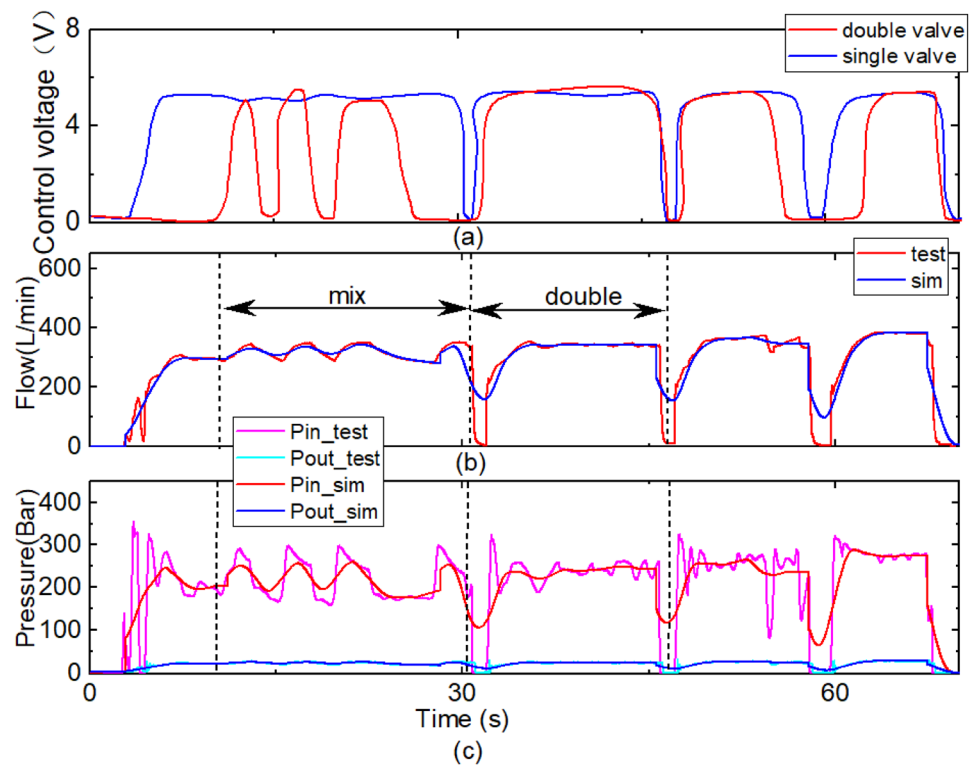
is cut. The acceleration of the hammer also reflects this characteristic.

The acceleration data of hammer body and frame in vertical direction is shown in Fig. 10a, and the corresponding SFT result is shown in Fig. 10b. As it can be seen from the Fig. 9, the amplitude of the acceleration in operating condition is smaller than the data in idle condition. For example, the amplitude of single and double mode in operating condition are  $190 \text{ m/s}^2$ , and  $200 \text{ m/s}^2$ , respectively, and the corresponding frequency are 32 and 41 Hz, which is smaller than the idle condition results in Sect. 3.2. Although the differences occurred during unsteady stages, dynamic characteristics of this hammer in steady stage, including mechanical and hydraulic parts, can be revealed with this coupled dynamic model.

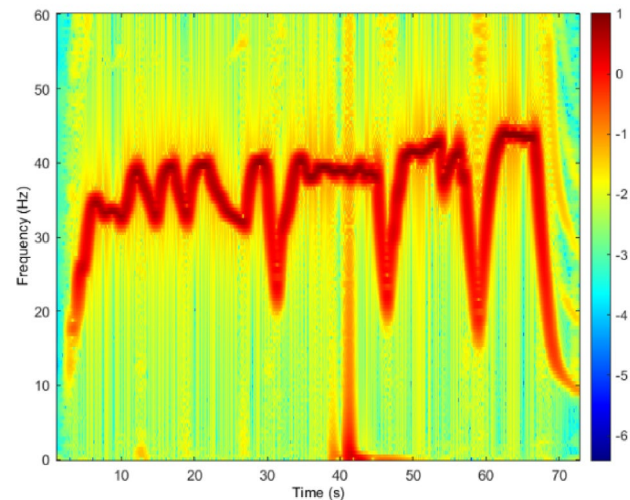
#### 4 Performance analysis and optimization

After verification of the coupled dynamic model, we analyzed the performance of the hammer with it. According to the experience in piling, the hammer in double mode would be more efficient than single mode. As it can be seen from the results in Sect. 3, the differences between double mode and single mode can be reflected by the frequency and amplitude of vertical acceleration. While the frequency is directly related to the speed of driving

**Fig. 9** Comparing results of flow and pressure in operating condition



(a) Acceleration data in operation condition



(b) SFT results of acceleration data

**Fig. 10** Acceleration and corresponding SFT results in operating condition

motor, which is decided by the inlet flow. Therefore, we can optimize the structure of eccentric mass to obtain better performance of the hammer, i.e., amplitude of vertical acceleration.

In order to indicate the involved parameters, the structure of eccentric mass is shown in Fig. 11. The dimension includes radius  $r$ , thickness  $\delta$ , and angle  $\alpha$ .

Due to the inside installation restrictions of hammer body, the radius is limited less than 175 mm, and the thickness is limited less than 190 mm, and the angle is unrestricted. We processed the simulation in idle condition with different radius, thickness, and angle based on the coupled dynamic model, and the inlet flow of

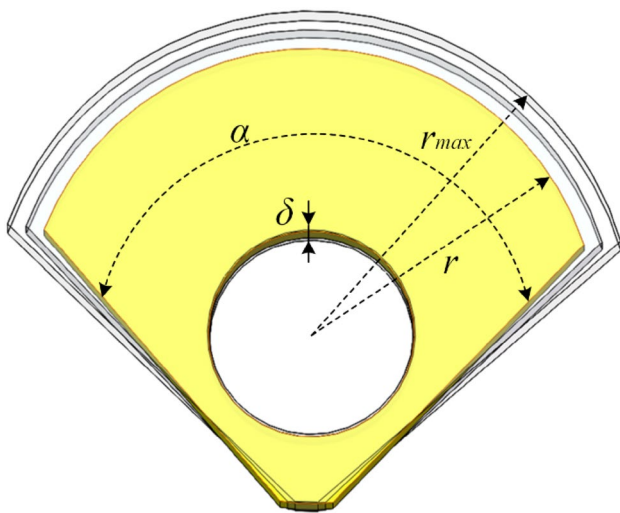


Fig. 11 Structure of eccentric mass

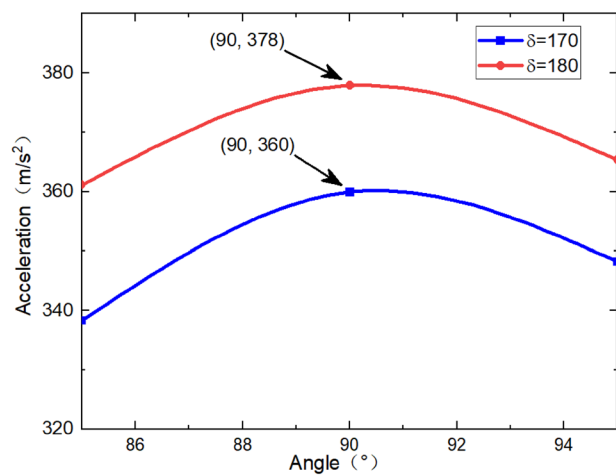
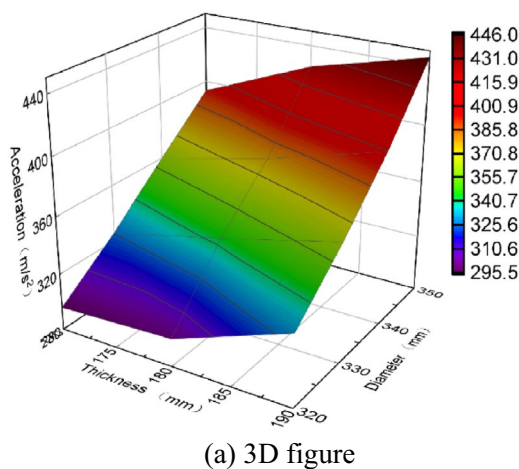
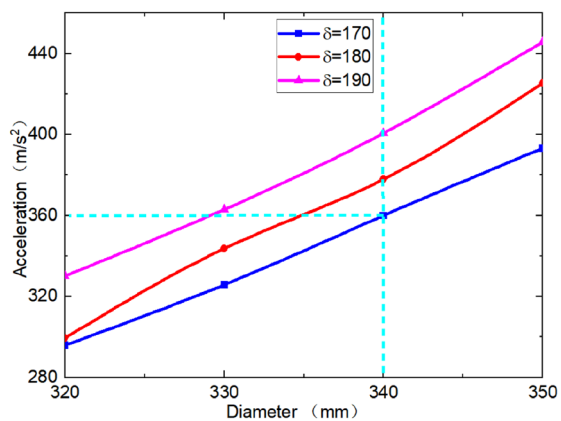


Fig. 12 Acceleration at different angle of eccentric mass



(a) 3D figure



(b) planar figure

Fig. 13 Acceleration at different diameter and thickness of eccentric mass

hydraulic motor is constant during the simulation. The results are shown in Figs. 12 and 13, respectively.

The hammer body acceleration at different thickness and angles is shown in Fig. 12. As it can be seen from Fig. 12, thicker eccentric mass would bring large amplitude of hammer body acceleration in vertical direction. According to Eq. (7), thicker eccentric mass would increase the mass, which will produce greater exciting force. And the increasing angle would bring a nonlinear change. When the angle is less than 90°, the acceleration increases with the increasing angle. While the acceleration decreases with the angle is greater than 90°. The maximum acceleration is obtained when the angle is 90°. The different angles not only change the mass of eccentric mass, but also change the eccentric distance, which is the key parameter in Eq. (7). The increasing angle produces different change trend for mass and eccentric distance, which brings the nonlinear characteristic.

The results of different radius and thickness is shown in Fig. 13. As it can be seen from details in Fig. 13a, the increasing thickness and radius would increase the amplitude of acceleration. However, the increasing radius bring more obvious change. According to Eq. (7), mass and eccentric distance are two key parameters. The thickness only increasing mass, while the increasing radius not only increase mass, but also increase the eccentric distance. And the trend of changes is same, which would bring more obvious increasing of acceleration.

According to the results in Fig. 13a and b, when the angle is 90°, thickness is 190 mm, and radius is 175 mm, the acceleration of hammer body is 440 m/s<sup>2</sup>, which is greater than 310 m/s<sup>2</sup>, obtained in Sect. 3 with field test. Although the amplitude of acceleration is monotonically changing with the diameter and thickness according to the results in Fig. 13, these results indicated the different

variation of acceleration when the thickness and diameter changed alone.

## 5 Discussion

According to above analysis, the dynamic responses of the hammer are the coupled results of mechanical parts, hydraulic parts, and workload. Therefore, the coupled dynamic model is crucial during the whole research, which is also the obvious difference between the model in this paper and previous researches [5, 6, 12]. We considered the coupled effects of mechanical parts, hydraulic parts, and also workload during piling process to establish the model. The model could be used to simulate the dynamic responses for different specification of hammers. And the hydraulic driving system results also indicated the power demand during the working process. The input power of the hammer in this paper under idle condition is about 47.3 kW and 136 kW for single and double mode. And the maximum power under operating condition is about 70 kW and 170 kW. The results would be useful during the power matching of excavator, i.e., the energy supplied machine and the hammer. Reasonable matching would bring about energy saving and efficiency.

Normally, the hydraulic hammer is used to pile under different soil conditions, much attention had been paid on the work efficiency under different soil conditions or workloads [11, 18]. The dynamic impact responses of the hammer including acceleration amplitude and frequency are the power source. Therefore, how to obtain better impact responses under different design parameters is very important. The separate evaluation of the impact responses was inaccurate and unreasonable without considering the hammer and workload. We optimized the hammer performance with the validated model, and better dynamic response can be obtained with the optimized parameters, i.e., the angle is 90°, thickness is 190 mm, and radius is 175 mm. The results and the model-based method can be used to evaluate the performance during design and use stage by changing the model parameters for the machine makers or users, and it will be more efficient and economy.

## 6 Conclusion

In order to evaluate the performance of hydraulic vibratory hammer economically and effectively, we proposed a model-based method in this paper. The accurate coupled dynamic model of the hammer, including mechanical model, hydraulic mode, and workload model, was established. The mechanical parts were considered as a 3

degrees of freedom (DOF) dynamic model, and the connections between the parts were modeled as springs and dampers. And the model was verified with field test of idle and operating conditions. However, during the operating condition of field test, the same pile hole was used, which meant that the work load in the field was smaller than the actual work load. Comparing results shown that the coupled dynamic model can reveal dynamic characteristics of the hammer in steady stage. The inlet flow of single and double mode changes with fluctuation, which is between 280 and 350 L/min. The corresponding inlet pressure changes between 15 and 29 MPa. The amplitude of single and double mode in operating condition are 190 m/s<sup>2</sup>, and 200 m/s<sup>2</sup>, respectively, and the corresponding frequency are 32 and 41 Hz. The working frequency of operating condition is lower than the idle condition. The practical value of the hammer may be different from the values in this paper owing to the difference of workload, while the dynamic trends would be useful during the performance evaluation of the hammer. Then we analyze the performance of the hammer with the coupled dynamic model, in which effects of different parameters of the eccentric mass on the vertical acceleration of hammer body are covered. Results show that acceleration amplitude is largest when the angle is 90°, and increasing thickness and radius bring powerful performance for the hammer. Considering the limitation of the field test, we will focus the effects of different work load during specific operating condition on the dynamic responses of the hammer in our future work.

**Funding** This research was funded by the National Natural Science Foundation of China (Grant number 52104159), the fellowship of China Postdoctoral Science Foundation (Grant No. 2021M690360), the National Key Research and Development Program of China (Grant No. 2016YFC0802900) for the financial support.

## Declarations

**Conflict of interest** On behalf of all authors, the corresponding author states that there is no conflict of interest.

**Open Access** This article is licensed under a Creative Commons Attribution 4.0 International License, which permits use, sharing, adaptation, distribution and reproduction in any medium or format, as long as you give appropriate credit to the original author(s) and the source, provide a link to the Creative Commons licence, and indicate if changes were made. The images or other third party material in this article are included in the article's Creative Commons licence, unless indicated otherwise in a credit line to the material. If material is not included in the article's Creative Commons licence and your intended use is not permitted by statutory regulation or exceeds the permitted use, you will need to obtain permission directly from the copyright holder. To view a copy of this licence, visit <http://creativecommons.org/licenses/by/4.0/>.

## References

1. Tavasoli O, Ghazavi M (2020) Driving behavior of stepped and tapered offshore piles due to hammer blows. *Mar Georesour Geotechnol* 38(6):633–646
2. Wang J, Yu J, Shiguo M et al (2016) Hammer's impact force on pile and pile's penetration. *Mar Georesour Geotechnol* 34(5):409–419
3. Qin Z, Chen L, Song C et al (2018) Field tests for investigating the extraction rate of piles using a vibratory technique. *J Shanghai Jiaotong Univ (Science)* 23(4):482–489
4. Karpenko M, Bogdevicius M (2020) Investigation into the hydrodynamic processes of fitting connections for determining pressure losses of transport hydraulic drive. *Transport* 35(1):108–120
5. Ruo C, Tang Z, Mo X et al (2019) Coupled synchronization capability of motor internal leakage of hydraulic vibratory hammer system without synchronous gear. *J Cent South Univ (Sci Technol)* 50(01):52–58
6. Qin Z, Chen L, Song C et al (2017) Field tests to investigate the penetration rate of piles driven by vibratory installation. *Shock Vib* 2017:1–10
7. Zhang Y (2013) Study of vibratory hammer's drive ability based on the hysteretic nonlinear resistance. *Dissertations*, Central South University
8. Luo T, Gan X, Luo W (2010) Nonlinear dynamics simulation of compacting mechanism with double-eccentric vibrator of asphalt-paver. In: 2010 International conference on intelligent computation technology and automation, vol 2010, pp 800–803. <https://doi.org/10.1109/ICICTA.2010.155>
9. Choluk R, ZhunHyok Z, ChungHyok C et al (2021) Optimization design analysis of the eccentric rotor system with SFD. *J Vib Eng Technol*. <https://doi.org/10.1007/s42417-021-00406-7>
10. Doshi S, Katoch A, Suresh A et al (2021) A review on vibrations in various turbomachines such as fans, compressors, turbines and pumps. *J Vib Eng Technol* 9:1557–1575
11. Liu G, Xu C (2008) Effect of amplitude modulation of hydraulic vibration hammer on piling efficiency. *J Wuhan Eng Inst* 1(01):13–16
12. Li H (2008) The Research on the pile driving vibration system of hydraulic vibration hammer modeling and simulation. *Dissertations*, Changsha University of Science and Technology
13. Zhou H (2014) Simulation of hydraulic vibratory hammer Based on AMESim. *Dissertations*, Dalian University of Technology
14. Hu J, Li L, Li K et al (2013) Energy-saving research of pile hammer based on pressure feedback. In: 2013 Fourth international conference on digital manufacturing and automation, (129), pp 545–549
15. Yin Y, Cai W (2019) Analysis of hydraulic hammer capacity under different inclination. In: 2019 2nd world conference on mechanical engineering and intelligent manufacturing, vol 2019, pp 164–168
16. Chen X, Zhai J, Zhang H et al (2020) Simulation study on unbalance vibration characteristics of dual-rotor system. *SN Appl Sci* 2:1423
17. Fotouhi M (2014) Dynamic soil-pile interaction by random vibration methods. *Dissertations*, Iowa State University
18. Gao J, Gao QC (2011) Influence of pile-soil-structure interaction on vibration control of a double-parts combined piling structures. *J Vib Eng* 24(4):421–427
19. Stosiak M (2015) The impact of hydraulic system on the human being and the environment. *J Theoretical Appl Mech* 53(2):409–420
20. Stosiak M (2014) Ways of reducing the impact of mechanical vibrations on hydraulic valves. *Arch Civil Mech Eng* 15(2):392–400
21. Grizi A, Athanasopoulos-Zekkos A, Woods RD (2016) Ground vibration measurements near impact pile driving. *J Geotech GeoEnviron Eng* 142(8):4016035
22. Song YP, Sun YF, Cao CL et al (2012) Study on Pile-Soil interaction during Pile Sinking and drivability of Pile in offshore platform. *Appl Mech Mater* 164:137–141
23. Khodair Y, Abdel-Mohti A (2014) Numerical analysis of Pile-Soil Interaction under axial and lateral loads. *Int J Concrete Struct Mater* 8(3):239–249
24. Wu JS, Chen CT (2007) Forced vibration analysis of an offshore tower carrying an eccentric tip mass with rotary inertia due to support excitation. *Ocean Eng* 34(8–9):1235–1244
25. Géradin M, Rixen D (1997) *Mechanical vibration: theory and application to structural dynamics*. Wiley, New York
26. Williamson D (1999) *Discrete-time signal processing*. IET, Stevenage

**Publisher's Note** Springer Nature remains neutral with regard to jurisdictional claims in published maps and institutional affiliations.